Faraday Discussions

Accepted Manuscript

This manuscript will be presented and discussed at a forthcoming Faraday Discussion meeting. All delegates can contribute to the discussion which will be included in the final volume.

Register now to attend! Full details of all upcoming meetings: http://rsc.li/fd-upcoming-meetings

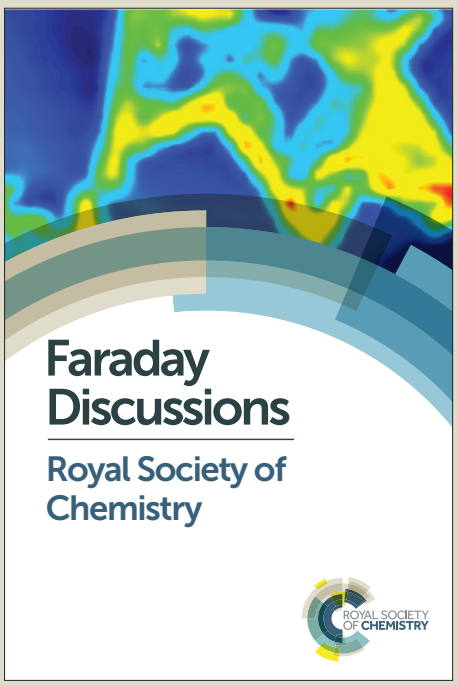

This is an *Accepted Manuscript*, which has been through the Royal Society of Chemistry peer review process and has been accepted for publication.

Accepted Manuscripts are published online shortly after acceptance, before technical editing, formatting and proof reading. Using this free service, authors can make their results available to the community, in citable form, before we publish the edited article. We will replace this *Accepted Manuscript* with the edited and formatted *Advance Article* as soon as it is available.

You can find more information about *Accepted Manuscripts* in the Information for Authors.

Please note that technical editing may introduce minor changes to the text and/or graphics, which may alter content. The journal's standard Terms & Conditions and the Ethical guidelines still apply. In no event shall the Royal Society of Chemistry be held responsible for any errors or omissions in this *Accepted Manuscript* or any consequences arising from the use of any information it contains.

ROYAL SOCIETY OF CHEMISTRY

www.rsc.org/faraday_d

Quantifying the formation of chiral luminescent lanthanide assemblies in aqueous medium through chiroptical spectroscopy and generation of luminescent hydrogels

Samuel J. Bradberry,[a] Aramballi Jayant Savyasachi,[a] Robert D. Peacock[b] and Thorfinnur Gunnlaugsson[a]*

[a] *School of Chemistry and Trinity Biomedical Sciences Institute, Trinity College Dublin, University of Dublin, Dublin 2, Ireland*

Fax: + 353 1 671 2826; Tel: + 3531 896 3459; gunnlaut@tcd.ie

[b] *School of Chemistry, University of Glasgow, Glasgow, G12 8QQ, Scotland, UK*

Abstract

Herein we present the synthesis and the photophysical evaluation of water-soluble chiral ligands (**2**·*(R,R)* and **2**·*(S,S)*) and their application in the formation of lanthanide directed self-assembled structures. These are pyridine-2,6-dicarboxylic amide based ligands, possessing two naphthalene moieties as sensitising antennae, that can be used to populate the excited state of lanthanides ions, were structurally modified using 3-propanesultone and caesium carbonate, allowing for the incorporation of a water-solubilising sulfonate motif. We show, using microwave synthesis, that Eu(III) forms chiral complexes in 1:3 (M:L) stoichiometries (**Eu**·[**2**·*(R,R)*]$_3$ and **Eu**·[**2**·*(S,S)*]$_3$) with these ligands, and that the red Eu(III)-centred emission arising from these complexes has quantum yields (Φ_{tot}) of 12% in water. Both circular dichroism (CD) and circular polarised luminescence (CPL) analysis shows that the complexes are chiral; giving rise to characteristic CD and CPL signatures for both the Λ and the Δ complexes, both possessing characteristic luminescence dissymmetry factors (g_{lum}), describing the structure in solution. The self-assembly process was also monitored *in-situ* by observing the changes in the ligand absorption and fluorescence emission, as well as in the Eu(III) luminescence. The change fitted using non-linear regression analysis demonstrated high binding affinity for Eu(III) which in part can be assigned to be driven by additional hydrophobic effects. Moreover, using CD spectroscopy, the changes in the chiroptical

properties of both (**2**·*(R,R)* and **2**·*(S,S)*) were monitored in real time. Fitting the changes in the CD spectra allowed for the step-wise binding constants to be determined for these assemblies; these matching well with those determined from both the ground and the excited state changes. Both the ligands and the Eu(III) complexes were then used in the formation of hydrogels; the Eu(III)-metallogels being luminescent to the naked-eye.

Introduction

The formation of metal-directed, self-assembled structures has been and remains a highly topical and major area of research within supramolecular chemistry.[1-4] Such supermolecules are structurally well-defined and ordered systems, designed and synthesised by using non-covalent chemistry.[5,6] The application of *d*-block metal ions to generate such supramolecular architectures has been well explored to date.[7-10] Often the physical properties of the metal ions, such as their magnetic[11] or photophyical[12,13] properties are also 'transferred' to the resulting structures resulting in the generation of novel functional nano-materials.[14] Many lanthanides possess important physical properties such as magnetic and photophysical properties; both of which have been well explored in the generation of novel and targeting imaging probes and sensors.[14,15]

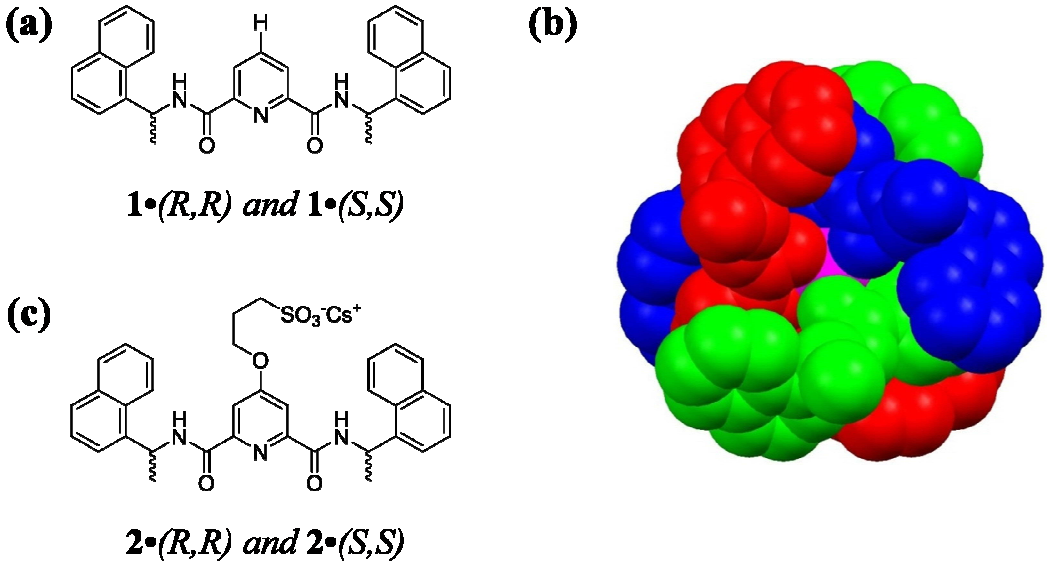

Figure 1. **(a)** The first examples of chiral **dpa** ligands possessing naphthalene antennae employed in the synthesis of lanthanide bundles. **(b)** The X-ray crystal structure of "Trinity Sliotars" using **1** and Eu(III). **(c)** Ligands **2**·*(R,R)* and **2**·*(S,S)* used in the current study, possessing propane sulfonate.

However, in contrast to *d*-metal ions, the use of *f*-metal ions to direct the synthesis of supramolecular structures or nano-structures, has been somewhat less explored to date,

but the lanthanides have high coordination requirements that are highly attractive .[15,16] Nevertheless, such exploration has resulted in the generation of some excellent examples. This includes the formation of coordination polymers or metal-organic frameworks (MOFs),[17] or of highly ordered supramolecular cages, bundles,[18] helicates,[19] and grids[20]. For some time now, we have been developing several examples where we used *f*-metal ion to direct the formation of self-assembly structures[21] such as bundles[22] or di-metallic-triple stranded helicates,[24] as well as generated the first example of [3]catenanes using lanthanide ion templation[25]. We have also employed various lanthanide ions in the generation of novel soft materials such as gels[26] and self-assembly mono-layers[27]. The self-assembly bundles, or "Trinity Sliotars", are examples of highly ordered lanthanide complexes from our laboratory consisting of 1:3 metal to ligand stoichiometry.[28] These ligands being based on the use of pyridine-2,6-dicarboxylic amides (**dpa**) derivatives, possessing chiral aryl chromophores, known as the sensitising antennae. An example of such structures is depicted in Figure 1a, using ligand **1**, with both the **1**·*(R,R)* and **1**·*(S,S)* giving rise to lanthanide bundles/complexes that were structurally characterised using X-ray crystallography (Figure 1b), and shown to be chiral. Moreover, the chirality of the ligand being transferred to the *f*-metal ion as demonstrated by employing circular polarised luminescence (CPL).[29] The photophysical properties of the ligands and the resulting complexes were successfully probed in various solvents, including CH_3CN and CH_3OH. However, attempts to monitor and analyse the *in-situ f*-metal directed formation in more competitive media, such as water or buffered aqueous solution, using **1** or related derivatives was not possible due to issues with solubility. Herein, we present ligands **2**·*(R,R)* and **2**·*(S,S)* (Figure 1c) which were designed to overcome this drawback; possessing grafted sulfonate functionality, that makes these ligands highly soluble in water, allowing us to probe the self-assembly behaviour in competitive media. Furthermore, we have recently shown the application of circular dichroism (CD) to monitor and quantify the formation of such assemblies in organic solution.[30] Herein, we demonstrate the use of CD spectroscopy to determine both the equilibrium processes and the binding affinities for the stepwise formation of such assemblies in water[31,32] where hydrophobic and metal coordination gives rise to large Cotton-effects in CD spectra. Moreover, we also demonstrate using CPL that the Eu(III)-centred emission from complexes made from both **2**·*(R,R)* and **2**·*(S,S)* is chiral as a consequence of the ion 'sitting' within a chiral ligand environment.

Results and Discussion

Synthesis of 2·*(R,R)* and 2·*(S,S)* and their corresponding Eu(III) complexes:

The synthesis of ligands **2**·*(R,R)* and **2**·*(S,S)* is shown in Scheme 1 (and detailed in the experimental section), starting from the commercially available chelidamic acid (**3**) which was reacted with *R*- or *S*-enantiomerically resolved 1-(1-naphthyl)ethylamine using peptide coupling methodology[23] (HOBt, EDCI and TEA in anhydrous THF) yielding the hydroxyl intermediate **3**·*(R,R)* and **3**·*(S,S)* as off-white solids in moderate yields after elution on silica (RediSep® 12g, 0 → 5 % MeOH in DCM). Synthesis of **2**·*(R,R)* and **2**·*(S,S)* was then achieved using synthetic methodology developed by O'Shea *et al.*[33] which involved the refluxing of the respective enantiomers of **5** with 1,3-propanesultone and caesium carbonate in anhydrous THF for two hours followed by concentration and sonication of the respective residues in acetone. Filtration of the resulting solids and thorough washing with acetone and diethyl ether gave crude products which could be purified from excess 1,3-propanesultone by reverse-phase (C-18) flash chromatography from which the desired products were recovered pure as caesium salts in 51% and 71% yields, respectively. Both ligands were characterised by standard methods (see ESI for further information) which included the use of ^{1}H NMR, ^{13}C NMR and IR spectroscopies, as well as high resolution ESMS; all confirming the formation of both **2**·*(R,R)* and **2**·*(S,S)*. Having successfully formed both **2**·*(R,R)* and **2**·*(S,S)* we next formed the Eu(III) complexes of these under microwave irradiation by

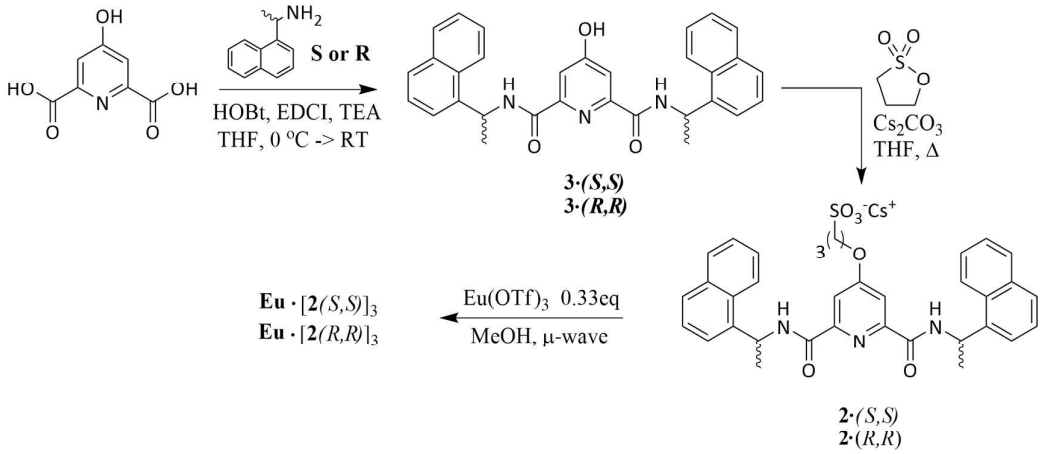

Scheme 1. Synthesis of **2**·*(R,R)* and **2**·*(S,S)*

treatment of the ligands with $Eu(CF_3SO_3)_3$ in 3:1 ratio in CH_3OH for 30 minutes followed by precipitation of the complexes from Et_2O. This gave **Eu**·[**2**·*(R,R)*]$_3$ and **Eu**·[**2**·*(S,S)*]$_3$ in 70 and 65 % yields, respectively. As above, these complexes were

characterised by conventional methods, including the use of NMR, IR, HRMS and elemental analysis. Both methods demonstrated the successful formation of these systems in 1:3 (metal:ligand) stoichiometry, where the HRMS (MALDI-TOF MS) showed the 1:3 species possessing isotopic distribution patterns that matched that of the calculated species.

Photophysical analysis of 2·*(R,R)* and 2·*(S,S)* as well as Eu·[2·*(R,R)*]$_3$ and Eu·[2·*(S,S)*]$_3$

The photophysical properties of **2**·*(R,R)* and **2**·*(S,S)* (c = 1 x 10^{-5} M) as well as the Eu(III) complexes, **Eu**·[**2**·*(R,R)*]$_3$ and **Eu**·[**2**·*(S,S)*]$_3$, were initially investigated in water, Figure 2. The absorption spectra of the ligands **2**·*(R,R)* and **2**·*(S,S)* were identical; showing a characteristic pyridine n $\rightarrow\pi^*$ (λ_{max} = 224 nm) and naphthyl $\pi \rightarrow\pi^*$ transitions, the latter possessing a fine structure consisting of bands at 275, 281 and 290 nm, respectively, Figure 2a for **2**·*(R,R)*$_3$. The spectra being structurally similar to that observed for **1**·*(R,R)* and **1**·*(S,S)* when recorded in organic solution. In both cases, the excitation of the long wavelength transition resulted in only very weak fluorescence emission, indicating significant quenching compared to that seen for related structures when recorded in organic solvents. In a similar manner both the absorption and the

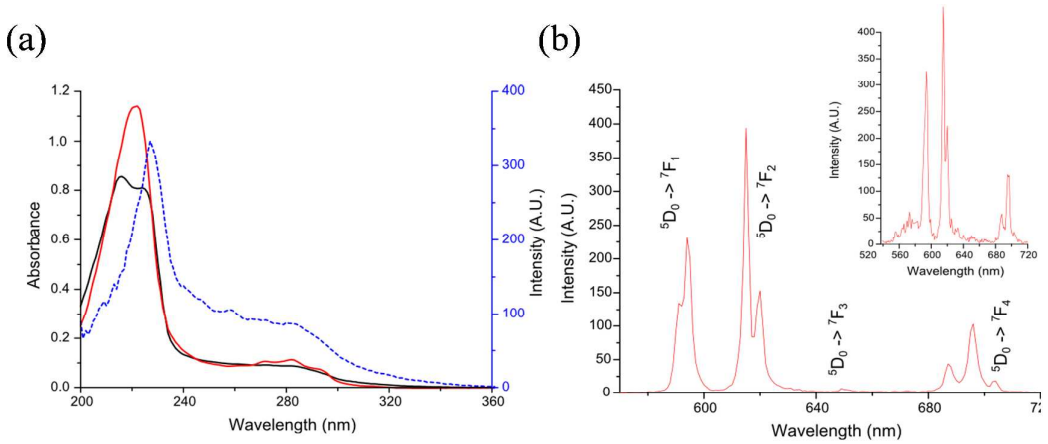

Figure 2. (a) UV-Vis absorbance spectra of **2.***(S,S)* (red) and **Eu**·[**2**·*(S,S)*]$_3$ (black). Excitation spectrum (λ_{em} = 615 nm) in phosphorescence mode (blue, dashed) **(b)** Phosphorescence spectrum of **Eu**·[**2**·*(S,S)*]$_3$ *Inset:* Fluorescence spectrum of Eu(III)-centred emission. All spectra recorded in H_2O at 24 °C; c = 1 × 10^{-5} M and 3.33 × 10^{-6} M for **2.***(S,S)* and **Eu**·[**2**·*(S,S)*]$_3$, respectively.

fluorescence emission spectra of the Eu(III) complexes were recorded in water, Figure 2a and 2b, respectively for **Eu**·[**2**·*(S,S)*]$_3$. Here, the absorption spectra showed hypochromic shifts at λ_{abs} = 220 and 281 nm with de-convolution of the pyridyl band

into two features, shifted by 5 nm - one red shifted (λ_{max} = 225 nm) and one blue shifted (λ_{max} = 215 nm). A concomitant hyperchromic shift of the region 300-310 nm demonstrated the conformational changes in solution and indicated complexation to the Eu(III) ion. The emerging Eu(III) centred emission at long wavelengths, Figure 2b, was assigned to $^5D_0 \rightarrow {}^7F_J$ (J = 0–4) and was clearly visible in the fluorescence emission, indicating that efficient sensitization of the Eu(III) excited state ($^5D_0$) by energy transfer from the ligands. The red Eu(III) emission was also clearly visible to the naked eye when irradiated under UV-light and long-lifetime emission was confirmed by observing the Eu(III)-centred emission in time-resolved spectroscopy (phosphorescence mode), as shown in Figure 2c, again for **Eu**·[**2**·*(S,S)*]$_3$. The ligand sensitisation was confirmed through the recorded excitation spectra (λ_{em} = 615 nm) which were found to be structurally similar to the absorption spectra of **Eu**·[**2**·*(S,S)*]$_3$, Figure 2d. Luminescence life-time (τ_{obs}) measurements for the Eu(III)-centred emission were also recorded in H_2O and D_2O (See ESI). The Eu(III) $^5D_0$ excited state life-times which were best fitted to monoexponential decay which indicated a single species in solution. These were determined as 1.6 ms in protic solvent and 3.9 ms in deuterated media. From this data, the hydration state, *q*, was determined as zero, using Parker's modified Horrock's equation for bound water molecules to Eu(III), indicating that the complexes had no aqua ligands coordinated to Eu(III).[34] The *q*-value of zero was consistent with the 1:3, Eu(III) to ligand, stoichiometry complex. The lifetimes were similar to those found for complexes of ligands such as **1.***(S,S)* and **1.***(R,R)* when recorded in aqueous suspension, which also gave hydration states of zero. The Eu(III) complexes of **2**·*(S,S)* and **2**·*(R,R)* were found to be stable in water and in buffered aqueous solution over a period of several months. The photoluminescence quantum yields (Φ_{tot}, %) were also determined as a standard in water, 0.1M HEPES buffer and in MeOH solutions using a relative method against Cs_3[Eu(**dpa**)$_3$]·9H_2O as the standard. The results are summarised in Table 1 and the values found to be significantly higher than that determined for **Eu**·[**1**·*(R,R)*]$_3$ and **Eu**·[**1**·*(S,S)*]$_3$ in CH_3CN and CH_3OH. For **Eu**·[**2**·*(R,R)*]$_3$ and **Eu**·[**2**·*(S,S)*]$_3$, the Φ_{tot} was determined as *ca.* 12% in both water and in buffer solutions, whereas in MeOH the Φ_{tot} was significantly less; being *ca.* 4%, which is similar to that seen for the complexes formed from ligand **1**.

We believe that the enhanced quantum yield efficiency in water is due to two factors. Firstly, the substitution on the 4-position of the pyridine ring with the alkoxy-moiety

might give rise to stronger donation of the pyridyl nitrogen to the Eu(III) ion (compare that seen in ligand **1**) and secondly, these are due to increased influence of hydrophobic effects from the amphiphilic nature of the ligand, which aids to exclude water from the coordination spheres of the Eu(III) ion and in turn influencing the efficiency of the sensitization. To evaluate this we determined η_{sens} (the parameter for antenna-to-ion energy transfer efficiency) for both **Eu**·[**2**·*(R,R)*]$_3$ and **Eu**·[**2**·*(S,S)*]$_3$. This was determined from τ_{obs} (in water or buffered solution), Φ_{tot} upon ligand excitation and the integrated intensity of ΔJ=2 fluorescence emission (see ESI for calculations) and showed large increase to 75 – 80 % in aqueous systems. This cannot be accounted for by the electronic effect of solvent polarity alone, with ground state features and behaviour in both water and MeOH being essentially equivalent. We therefore propose that the amphiphilic nature and hydrophobically driven assembly in aqueous solution enhances the antenna-to-ion energy transfer efficiency.

The absorbance and emission features were also recorded in buffered (0.1 M HEPES) water and were found to be consistent with neat water. Lifetimes in buffered H_2O and D_2O were also measured, which again matched that seen in water, and in a similar manner the Φ_{tot} were recorded in buffered solution and were shown to be similar, Table 1. The ionic strength was therefore not having a substantial quenching effect on the luminescence; indeed, neither did it appear to have a substantial effect on the self-assembly processes, as characterised though the lifetimes recorded.

Table 1. Photophysical parameters for Eu(III) complexes of **2**·*(R,R)* and **2**·*(S,S)* self-assembled in solution in various solvents. Overall experimental luminescence quantum yields (Φ_{tot}), antenna-to-ion transfer efficiencies (η_{sens}), observed luminescence lifetime (τ_{obs}) measured at 24 ˚C and calculated radiative lifetime (τ_R) and Φ_{Ln}^{Ln} (See ESI for equations).

Complex	Solvent	τ_{obs}, ms	Φ_{tot}, %	τ_R, ms	Φ_{Ln}^{Ln}, %	η_{sens}, %
Eu·[**2**·*(S,S)*]$_3$	H_2O	1.59(2)	11.4(3)	11.0(2)	14.5(3)	78.5(4)
	0.1M HEPES	1.58(1)	10.9(5)	11.4(1)	13.9(3)	78.0(4)
	MeOH	1.62(1)	4.5(3)	12.7(4)	12.8(3)	35.0(2)
Eu·[**2**·*(R,R)*]$_3$	H_2O	1.60(1)	11.8(3)	9.5(3)	16.9(4)	69.6(4)
	0.1M HEPES	1.58(2)	11.6(4)	10.4(3)	15.2(4)	76.6(3)
	MeOH	1.68(2)	3.4(2)	12.9(2)	13.0(2)	26.4(2)

The chirality of both the ligands and the Eu(III) complexes was confirmed by using CD

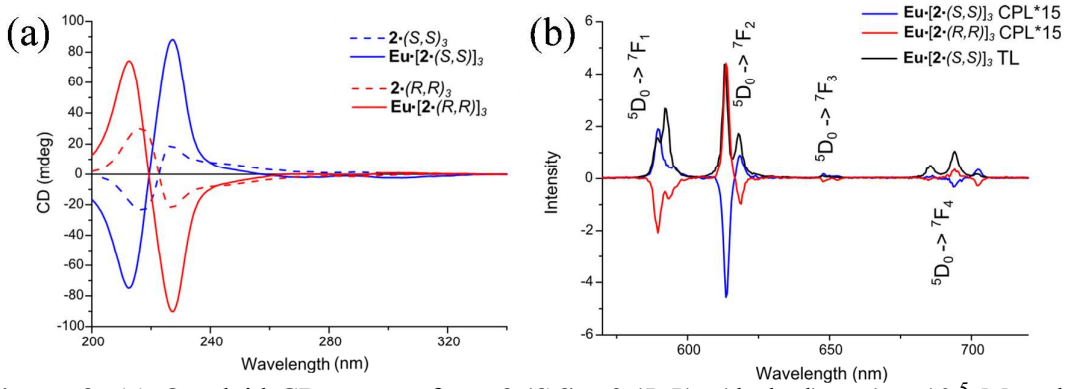

Figure 3. **(a)** Overlaid CD spectra from **2.**$(S,S)_3$, **2.**$(R,R)_3$ (dashed) at 1×10^{-5} M and **Eu·**[**2**·*(R,R)*]$_3$, **Eu·**[**2**·*(S,S)*]$_3$ (solid) at 3.3×10^{-6} M in water at 24 °C **(b)** CPL and Total Luminesence (TL) spectra recorded for **Eu·**[**2**·*(R,R)*]$_3$, **Eu·**[**2**·*(S,S)*]$_3$ in water.

and CPL spectroscopy in water. The results were consistent with the presence of a single chiral stereoisomer in solution for both ligands and their complexes. The CD spectra of the ligands **2**·*(R,R)* and **2**·*(S,S)* are presented in Figure 3a. As expected they were mirror images, with transitions of equal magnitude by opposite signs. Moreover, these CD spectra possess Cotton effect and can be characterised by Davydov splitting of 6 and 5 nm.[35] The complexes also showed clear Cotton effects, giving, as in the case of the ligands, rise to equal but opposite dichroism bands. The CD spectra of **Eu·**[**2**·*(R,R)*]$_3$, **Eu·**[**2**·*(S,S)*]$_3$ possess very different structure compared to the ones observed for their corresponding ligands, with small but measurable increases in the Davydov splitting to 6 and 7 nm alongside the enhancements in intensity. As intense bisignate CD Cotton effects was also observed for both complexes, which would indicate a coupling between the naphthyl antennae we recorded the CD spectra of both Eu(III) complexes as a function of temperature (See ESI). Varying the temperature from –10 to 50 °C only resulted in minor enhancement in the CD signals for both systems as Eu(III) complexes, the ligand CD showed measurable, but still small, intensity and wavelength shift.

The chiral environment of the Eu(III) ion was subsequently probed by recording the CPL spectra upon excitation into the ligand absorption bands. The chiral nature of such coordination complexes and assemblies may be transferred to the Eu(III)-centred emission in the formation of enantiopure bundles that place the metal ion in to a highly chiral environment. This was indeed found to be the case and the Eu(III) emission gave

rise to mirror-image CPL spectra showing the appearance of $^5D_0 \rightarrow {}^7F_J$ (J = 0–4) transition bands, Figure 3b.

The CPL spectra of both **Eu·[2·*(R,R)*]$_3$**, **Eu·[2·*(S,S)*]$_3$**, were structurally identical to that observed for "Trinity Sliotar" complexes; the CPL of **Eu·[2·*(S,S)*]$_3$**, or the **Δ** complex, showed a positive CPL for the ΔJ = 1 and 3 bands, while the ΔJ = 2 and 4 bands are split and give bisignate CPL signals with positive and negative components. The distribution of CPL signals as positive or negative may act as a structural signature for the absolute complex stereochemistry in solution having studied a family of "Trinity Sliotar" complexes with a variety of spectroscopies, including X-ray diffraction data of solid state structure.[28] **Eu·[2·*(R,R)*]$_3$** was confidently assigned as the **Λ** complex and **Eu·[2·*(S,S)*]$_3$** as **Δ**. The CPL distribution was found to be consistent with previously characterised "Trinity Sliotar" complexes for **Eu·[2·*(R,R)*]$_3$**, **Eu·[2·*(S,S)*]$_3$**, and therefore confirmed confidently that in the aqueous environment complex geometry is not affected by the competitive environment. Luminescence dissymmetry factors g_{lum}, were calculated for all of these transitions (see SI) from the ratio of CPL to total luminescence (TL) through the relationship shown in equation (i):

$$g_{lum} = \frac{2.(CPL)}{TL} \quad \text{(i)}$$

The CPL signals are relatively weak overall with dissymmetry factors (g_{lum}) of various magnitudes calculated for the different $^5D_0 \rightarrow {}^7F_J$ transitions calculated. Selected g_{lum} values are presented in Table 2, they are comparable to those typically seen for emissive enantiopure Eu(III) and Tb(III) complexes where g_{lum} is observed between 0.1 and 0.5. For $^5D_0 \rightarrow {}^7F_1$ (589 nm) were found to be 0.16 and –0.15, while for $^5D_0 \rightarrow {}^7F_2$ (615 nm);

Table 2. Selected g_{lum} values calculated (using equation (i)) from the Eu(III) transitions in CPL spectra of **Eu·[2·*(R,R)*]$_3$** and **Eu·[2·*(S,S)*]$_3$** recorded in H_2O.

λ_{em}	**Eu·[2·*(S,S)*]$_3$** g_{lum}	**Eu·[2·*(R,R)*]$_3$** g_{lum}	**Transition**
589	0.16	-0.18	$^5D_0 \rightarrow {}^7F_1$
614	-0.14	0.13	$^5D_0 \rightarrow {}^7F_2$
618	0.07	-0.08	
652	0.24	-0.24	$^5D_0 \rightarrow {}^7F_3$
685	0.03	-0.02	$^5D_0 \rightarrow {}^7F_4$
694	-0.04	0.05	
702	0.31	-0.22	

these are relatively large within the "Trinity Sliotar" family and the magnitude, in addition to sign, reflect the solution geometry and stereochemistry, as expected.

Observing the formation of Eu·[2·*(R,R)*]$_3$, Eu·[2·*(S,S)*]$_3$ *in situ*

Having analysed the various photophyhiscal properties of the ligands and complexes above, we next investigated the self-assembly process between the ligands and Eu(III) in water. The speciation from the Eu(III)-directed self-assembly was monitored by multiple spectroscopic methods in parallel using UV-vis absorbance, fluorescence and time-gated luminescence spectroscopies.

We first evaluated the solution stability **Eu·[2**·*(R,R)*]$_3$, **Eu·[2**·*(S,S)*]$_3$ in water. Despite the formation of charge neutral complexes at 1 × 10^{-5} M, both remained stable in solution and fully soluble in water. However, at higher concentrations evidence of precipitation was observed; consequently, all spectroscopic titrations were carried out at this concentration. At this concentration the lanthanide directed self-assembly was also observed to be fast (no equilibrium period was needed) and hence, the ligand solutions (c = 1 × 10^{-5} M) were titrated by sequential additions of aqueous Eu(OTf)$_3$ and the spectra at each addition recorded. The overall changes in absorbance spectra are shown

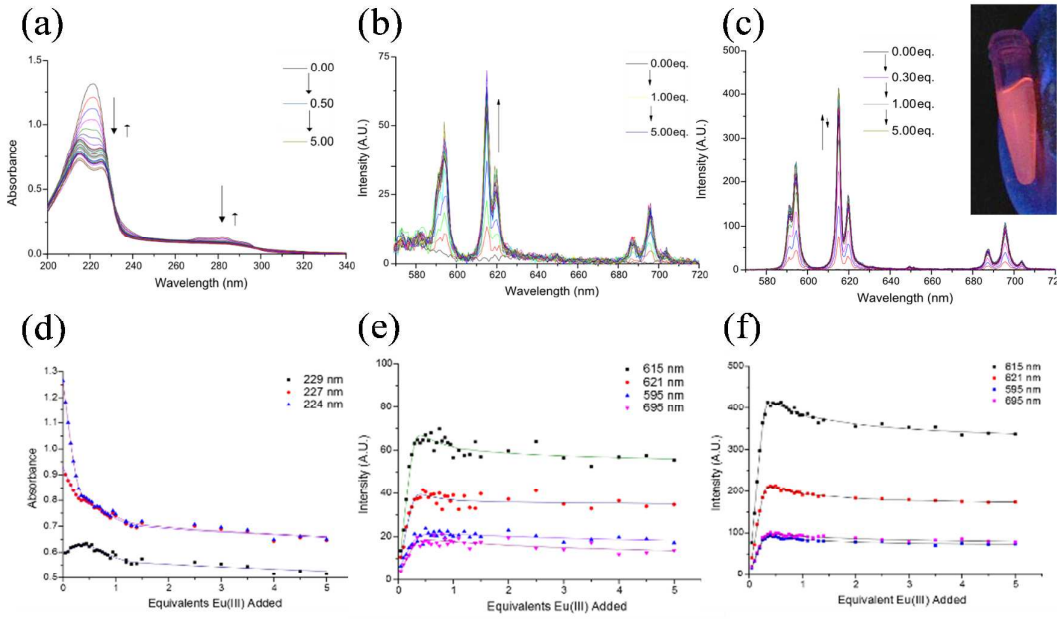

Figure 4. Spectra recorded from the titration of **2**·*(S,S)* with Eu(OTf)$_3$ at c = 1 × 10^{-5} M in H_2O at 24 °C from **(a)** UV-Vis absorbance **(b)** Fluorescence **(c)** Phosphorescence; Associated spectral changes (points) and regression fits (lines) plotted as a function of Eu(III) equivalents for **(d)** UV-Vis absorbance **(e)** Fluorescence emission **(f)** Phosphorescence emission.

in Figure 4a.

Here the main changes were observed in the naphthyl $\pi \rightarrow \pi^*$ transitions at 270-300 nm, and in the higher energy $n \rightarrow \pi^*$ transitions at 220 nm. An enhancement in absorbance at longer wavelength was observed, with a clear isosbestic point appearing at 291 nm. Analysis of these changes as a function of added Eu(III) equivalents, demonstrated that the main changes in the absorption spectra occurred within the addition of 0.3 equivalents of Eu(III) and that only relatively minor changes occurred at higher equivalents of Eu(III) (0.3 → 4 equivalents). The relatively minor quenching of Eu(III)-centred luminescence after 0.3 equivalents of Eu(III) was unlike that seen for the formation of **Eu**·[**2**·*(R,R)*]$_3$, **Eu**·[**2**·*(S,S)*]$_3$where emission rapidly diminishes upon the formation of 2:1 and 1:1 species dominantly in solution. Consequently, one can assume that this difference is due to the solvent affect where the more hydrogen bonding and competitive water media gives rise to additional hydrophobic effects that while favouring the formation of the 1:3 stoichiometry initially also subsequently stabilises the luminescence of the other stoichiometries, and this will be discussed in greater detail further below.

As discussed above, the ligand was found to only give rise to weak fluorescence and the changes in the ligand based emission could not be used to monitor the formation of either **Eu**·[**2**·*(R,R)*]$_3$, **Eu**·[**2**·*(S,S)*]$_3$. However, upon titration with the Eu(III) salt, in phosphorescence mode (time-gated luminescence) the evolution of the Eu(III)-centred emission with the intensity enhancement of the characteristic Eu(III) transitions $^5D_0 \rightarrow {}^7F_J$ occurring at 585, 616, 621 and 700 nm, Figure 4c was observed. In fact, the evolution of metal centred emission was also observed in the fluorescence mode, Figure 4b. The red emission was also visible to the naked eye at this low concentration upon placing the solution under a UV-Vis lamp with excitation wavelength of 360 nm, Figure 4e as inset. Comparing these results with the changes observed in both the absorbance and emission spectra upon self-assembly of the "Trinity Sliotar" from **1**·*(R,R)* and **1**·*(S,S)*, that were carried out in either CH_3CN or mixture of CH_3CN-CH_3OH solutions, showed that the naphthyl $\pi \rightarrow \pi^*$ transitions were much smaller in magnitude while the splitting for the 220 nm band into two separate features (pyridyl and naphthyl $n \rightarrow \pi^*$) was considerably more evident. This substantially influenced our ability to fit a model to this data, as shall be discussed below. Similarly, the sensitised-emission from the Eu(III) centre was observed to evolve immediately and increase to reach a maximum at 0.3

equivalents which is consistent with the expected 1:3 stoichiometry formation. Nevertheless, upon further additions of Eu(III) (up to 5 equivalents), the decrease in sensitised Eu(III) centred emission was much less than observed for that seen for complexes made from **1**·*(R,R)* and **1**·*(S,S)*; as these were found to quench more rapidly above the addition of one equivalent of metal ion. This we propose is due to combined hydrophobic effect and the amphiphilic nature of **2**·*(R,R)* and **2**·*(S,S)* which possibly is might giving rise to hydrophobically driven processes of assembly and solvation that exclude and limit the exposure of H_2O quenchers to the unsaturated Eu(III) centre; a phenomenon that is also evident from the quantum yield measurements above.

As can be seen from the results above, significant changes were seen in the CD spectra of the ligand upon complexation to Eu(III). Consequently, we also monitored the formation *in situ* using CD spectroscopy in real time. However, titrations were completed in pure water and not in buffered solution to retain the important features of

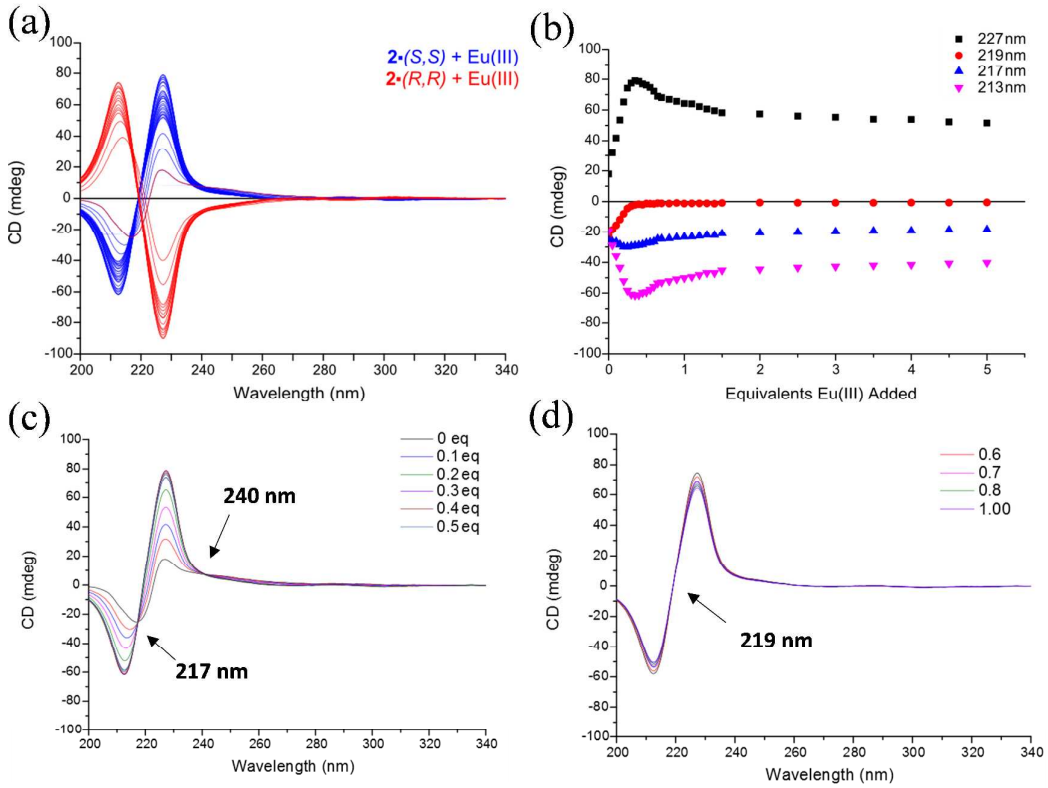

Figure 5. (a) CD titrations of **2**·*(R,R)* and of **2**·*(S,S)* with $Eu(OTf)_3$; c = 1 × 10^{-5} M in H_2O at 24 °C. **(b)** CD changes plotted as a function of Eu(III) equivalents for λ = 213, 217, 219 and 227 nm **(c)** CD spectra from titration of **2**·*(S,S)* between 0→0.5 equivalents Eu(III) **(d)** CD spectra from titration of **2**·*(S,S)* between addition of 0.60→1.00 equivalents Eu(III)

chiral absorbance between 200 – 220 nm, which are disrupted by scattering in HEPES or

TRIS buffered systems. The titrations were carried out in an identical manner to that above and at the same ligand concentration. The enantiopure **2**·*(R,R)* and **2**·*(S,S)* ligands showed opposite CD features with large elipticity of the 224 nm centred absorbance and minor signal for the naphthyl $\pi \rightarrow \pi^*$ transitions at 275 nm. As discussed previously, they showed equivalent substantial changes upon the addition of Eu(III). The overall titration is shown in Figure 5a for **2**·*(S,S)*.

As can be seen the overall changes were of equal but opposite dichroism bands confirming the presence of a single enantiomer in solution for these systems. Here, an instantaneous enhancement in both Cotton effect bands in the bisignate feature at 210-230 nm was observed upon titration with Eu(III); with a further enhancement and the emergence of isoeliptic points at 217 and 240 nm, Figure 5b. For these titrations, maxima were reached in both the positive and negative Cotton bands upon the addition of 0.30 equivalents of Eu(III) which is consistent with the formation of the desired 3:1 complexes, Figure 5c. Upon further additions of Eu(III) a second isoeliptic point occurring at 219 nm, with decrease in CD signal to plateau, was observed for both ligands at Eu(III) equivalents greater than one. This is consistent with a shift in the equilibrium processes towards the dissociation of 3:1 complexes into 2:1 and eventually the formation of 1:1 species for both ligands, which we determined by modelling and quantifying the binding.

Quantifying the binding affinity of 2·*(R,R)* and 2·*(S,S)* with Eu(III) using changes in the absorption and emission spectra

The spectral changes observed in both the absorption and the emission spectra in water were analysed through non-linear regression using a global analysis multiple regression to model the entire spectrum simultaneously (ReactLab EQUILIBRIA®). This allowed us to determine both the binding constants (expressed as $\log\beta_{M:L}$) and the various stoichiometries (equilibrium processes) in solution. The binding constants determined from these analyses are summarised in Table 3.

We first analysed the changes observed in the absorption spectra. Initial modelling of the changes, Figure 4a, in the long wavelength naphthalene absorption gave equilibrium models consisting of three species: **L**, **M:L** and **M:L$_3$**. However, we were also able to fit the data using the four species model: **L**, **M:L**, **M:L$_2$** and **M:L$_3$**. The reason for this is most likely due to lower sensitivity of the naphthyl $\pi \rightarrow \pi^*$ transitions and relatively small overall changes seen in the naphthalene absorption with the main changes in the

Table 3. Binding constants ($\log\beta_{M:L}$) obtained by fitting the changes in UV-Vis absorbance, time-gated luminescence (phosphorescence) and CD absorbance from titration data of **2**·*(R,R)* and **2**·*(S,S)* in H_2O at 23°C.

	2· *(S,S)*			**2**· *(R,R)*		
	$\log\beta_{1:1}$	$\log\beta_{1:2}$	$\log\beta_{1:3}$	$\log\beta_{1:1}$	$\log\beta_{1:2}$	$\log\beta_{1:3}$
UV-vis	7.4 ± 0.1	12.2 ± 0.1	19.1 ± 0.1	7.5 ± 0.1	14.4 ± 0.2	18.9± 0.2
Phosph.	6.1 ± 0.1	12.1 ± 0.1	18.7 ± 0.1	5.8 (fix)	12.0 ± 0.1	17.1± 0.1
CD	7.0 ± 0.1	13.4 ± 0.1	19.7 ± 0.1	5.8 ± 0.1	12.1 ± 0.1	17.3 ± 0.1

absorption spectra occurring at the higher energy pyridyl transition. The analysis of these changes subsequently became more challenging. In fitting these changes, good fits were however obtained, Figure 4d, and we were able to determine both $\log\beta_{1:1}$ and $\log\beta_{1:3}$ as major species; the binding constant being calculated as approximately 7 and 19, respectively. This affinity is of similar magnitude to that seen for the analysis of **Eu**·[**1**·*(R,R)*]$_3$ and **Eu**·[**1**·*(S,S)*]$_3$. From this analysis we were able to construct a speciation distribution diagram for the self-assembly of **2**·*(R,R)* and **2**·*(S,S)*, with Eu(III), which showed that the **M:L$_3$** stoichiometry is primarily formed at the beginning of the titration, but to a lesser extend, *ca.* 45%, than seen for **1**·*(R,R)* and **1**·*(S,S)* in organic solvents such as CH_3CN (See ESI), which gave rise to formation of *ca.* 70-90%.[23] This we assign to more competitive media and the hydrophobic effect not simply directing the formation of the 1:3 assemblies, but rather stabilising other stoichiometries by promoting intermolecular interaction that gives rise to formation of other self-assemblies such as the **M:L$_2$** and **M:L**. The latter of these was present in solution at 0.3 equivalent of Eu(III) in *ca.* 25%, alongside the dominant 1:3, while the remaining speciation was accounted for by free ligand **L** and only a small amount of the 1:2 complex **M:L$_2$**. Then at higher Eu(III) concentrations, the 1:1 complex (for both ligands) is the main species in solution with 1:2 being present but never dominating the complex stoichiometries in aqueous media.

Given the relatively small changes observed in the absorption spectra, the analysis of the Eu(III) centred emission gave more reliable results, particularly in relation to analysis of the 1:2 complexes, due to the significantly larger changes observed. The fitting of the data for the $^5D_0 \rightarrow {}^7F_J$ (J = 0–4) transitions are shown in Figure 6a; with the corresponding speciation distribution diagram being shown in Figure 6b. Good fitting for all the $^5D_0 \rightarrow {}^7F_J$ (J = 0–4) transitions was observed using the **M:L**, **M:L$_2$** and **M:L$_3$** model. As was seen for the changes in the absorption spectra, the **M:L$_3$** stoichiometry was initially formed, but unlike that seen above, the **M:L$_2$** stoichiometry was also

prominent. From these the binding constants 6.1 ± 0.1, 12.1 ± 0.1 and 18.7 ± 0.1 were determined for $\log\beta_{1:1}$, $\log\beta_{1:2}$ and $\log\beta_{1:3}$, respectively, matching well with that observed previously in our laboratory. The results from both the ground and the Eu(III) excited state clearly show that the results can be modelled to give binding constants that show good correlation in their magnitude, while the speciation distribution is somewhat different; particularly as the **M:L$_2$** is not easily identified in the absorption spectra. To address this we also investigated the changes observed in the CD spectra.

Quantifying the binding affinity of 2·*(R,R)* and 2·*(S,S)* with Eu(III) using chiroptical changes

To better assess the conclusion of the three *vs*. a four-component model discussed above, we also analysed the changes observed in the CD spectra. While using chiroptical changes to investigate the binding interactions of biomolecules with drug candidates, such as DNA and Ru(II) polypyridyl complexes,[36] is well documented, then to the best of our knowledge, only very few reports have to date focused on studying the self-assembly between chiral organic ligands and lanthanide ions in solution.[37] The use of CD is highly attractive for exploring or accessing vital information about equilibrium processes as potentially changes can be both significantly large than that seen in

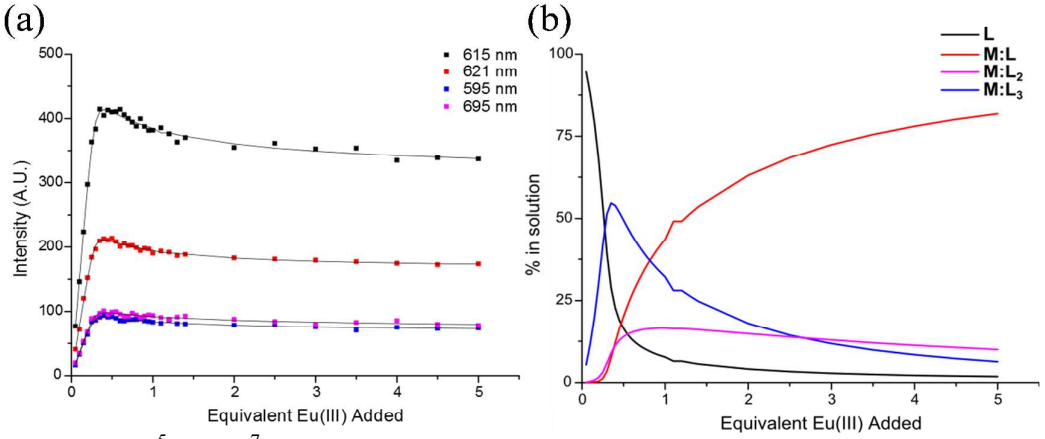

Figure 6. (a) $^5D_0 \rightarrow {}^7F_J$ intensity changes plotted as a function of Eu(III) equivalents (points) and their respective binding isotherms calculated from non-linear regression analysis in ReactLab EQUILIBRIA® (lines) **(b)** Speciation diagram generated from the modelling of the titration data for **L**, **M:L**, **M:L$_2$ and M:L$_3$**

conventional UV-Vis absorption spectroscopy and secondly, the spectra representing a particular stoichiometry should have a CD signature that is unique to that structure and can be used as a fingerprint or a signature for each of the stoichiometries in solution. Recently, we have shown that probing changes in the chiroptical properties of lanthanide

self-assembled lanthanide structures from chiral ligands and fitting the data using non-linear regression analysis can indeed allow for additional information to be revealed that can help in furthering elucidation of the stoichiometry, the binding constants and the speciation distributions of such self-assemblies in solutions. The analysis of the CD-spectra initially shown in Figure 3, is particularly attractive from the point that the changes in the CD spectra, Figure 5, are significant as is evident from the titration itself.

As demonstrated in Figure 5b, the changes in the CD spectra of both **2**·*(R,R)* and **2**·*(S,S)* were significant upon binding to Eu(III). Plotting the changes as a function of added Eu(III) resulted in binding isotherms that showed three clear binding events. Here, the largest changes were seen up to the addition of 0.3 equivalents of Eu(III); with further changes occurring until 0.5 and 1 equivalents, respectively, Figure 7a for all the different transitions observed for both enantiomers. Furthermore, the observation of sequential isoepliticity during titration between the key points of 0 → 0.3, 0.3 → 0.5 and 0.5 → 1 equivalents of Eu(III) all demonstrated the presence of multiple species and multiple pairs of correlated species in solution, Figure 5a-c. Fitting the data to the binding model consisting of **L**, **M:L**, **M:L$_2$** and **M:L$_3$** indeed gave excellent fit as is demonstrated in Figure 7a. This, in fact, gave greater confidence to our conclusions of

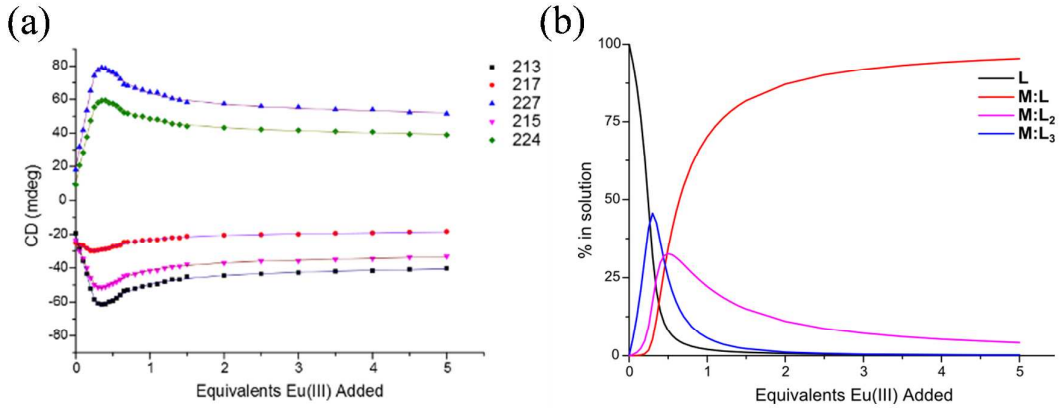

Figure 7. (a) Changes in key CD spectra features for the assembly of complexes of **1**·*(S,S)* at c = 1 × 10^{-5} M (points) and their respective binding isotherms calculated from non-linear regression in Reactlab EQUILIBRIA® (lines) **(b)** Speciation diagram generated from the modelling of the titration data for **L**, **M:L**, **M:L$_2$** and **M:L$_3$**.

the existence of four total species in solution, including the presence of **M:L$_2$** which we could not identify with great confidence from the fitting of the changes in the absorption spectra above. The speciation was recalculated using the chiral absorbance data and supports the formation of a greater percentage of 1:2 complex in solution throughout the titration, Figure 7b. In fact, fitting of the changes seen in the CD spectra specifically did

not support the model where **M:L$_2$** was excluded; consistent with the best fit models derived from emission spectroscopies. From these fittings we were able to determine the binding constants log$\beta_{1:1}$, log$\beta_{1:2}$ and log$\beta_{1:3,}$ as 7, 13 and 19 ± 0.1, respectively, for the **2**·*(S,S)* enantiomer, with similar results being seen for **2**·*(R,R)*. These values compare well with that seen above using the more 'classical' approach of fitting the changes in the absorption and emission spectra. Using this information we also calculated the CD spectra of the various species in solution (see ESI). These clearly showed that each of the **M:L**, **M:L$_2$** and **M:L$_3$** models have characteristic spectra that can be looked at as 'fingerprints' for each species in solution. These reflected the Cotton band shifts, splitting of each species and clearly demonstrate the largest enhancement for the highly bundled **M:L$_3$** species. Such analogy is commonly done with changes observed in the absorption spectra; however, in our case, the changes are relatively small, while the corresponding changes in the CD spectra are significant, demonstrating the potential use of chiral spectroscopy, specifically CD, in monitoring and quantifying the formation of supramolecular structures in metal ion directed synthesis from chiral ligands.

Synthesis and characterisation of 2·*(S,S)* and Eu(III) hydrogels

Having generated both **Eu**·[**2**·*(R,R)*]$_3$ and **Eu**·[**2**·*(S,S)*]$_3$ and investigated the self-assembly between the ligands **2**·*(R,R)* and **2**·*(S,S)* with Eu(III) *in situ*, we next explored the potential application of these ligands and complexes in the generation of novel responsive soft-materials. While all the above experiments were carried out at low

Figure 8. (a) Ligand hydrogels formed of **2**·*(S,S)* at 6 wt% (left) and 10 wt%. **(b)** Ligand hydrogels formed at 6 wt% (left), 10 wt% (middle) and Eu(III)-doped 5 wt% hydrogel, under ambient light **(c)** under UV light (λ = 254 nm).

concentration, where these structures exists as discreet molecular assemblies, then at concentration higher than 1 × 10^{-5} M, both ligands formed hydrogels as demonstrated in Figure 8a. The critical "gelation", or aggregation concentration in water was determined as 6 wt%, in the presence of Cs_2CO_3 upon heading. This method produced gels of varying transparency dependent on wt% of **2**·*(S,S)* and the Cs_2CO_3 salt content in a

consistent manner; resisting the inversion test as shown in Figure 8a. The resulting materials were shown to be clear and opaque at 6 and 10 % w/w, respectively, and when exposed to UV light (λ =254 nm) both emitted with blue fluorescence, Figure 8c, characteristic of that seen for the ligand alone.

The introduction of Eu(III)-triflate salt to these gels by layering a solution of the Eu(III) salt on top of the gel material, produced initially materials that were characteristically red luminescent as demonstrated in Figure 8c **Eu**·[**2**·*(S,S)*]$_3$. However, upon aging (over the period of few hours), these metallogels were shown to be unstable, as the Eu(III) complexes began to precipitate within the gel matrix, resulting in phase transition from gel to sol. The complex, once formed within the gel, was overall charge neutral and this most likely caused the precipitation process form the gel matrix to occur. Using other Eu(III) salts such as chloride and acetate gave the same result; the layering of salt solution initiating the phase transition. The Eu(III) based materials were too unstable to allow for in-depth morphological analysis using scanning electron microscopic (SEM) imaging; however, such analysis could be carried out on the ligand hydrogels. This is in contrast to that recently observed in our laboratory where Eu(III) gels formed from simple **dpa** ligands formed highly organised fibrous gels which were both luminescent and healable.[26]

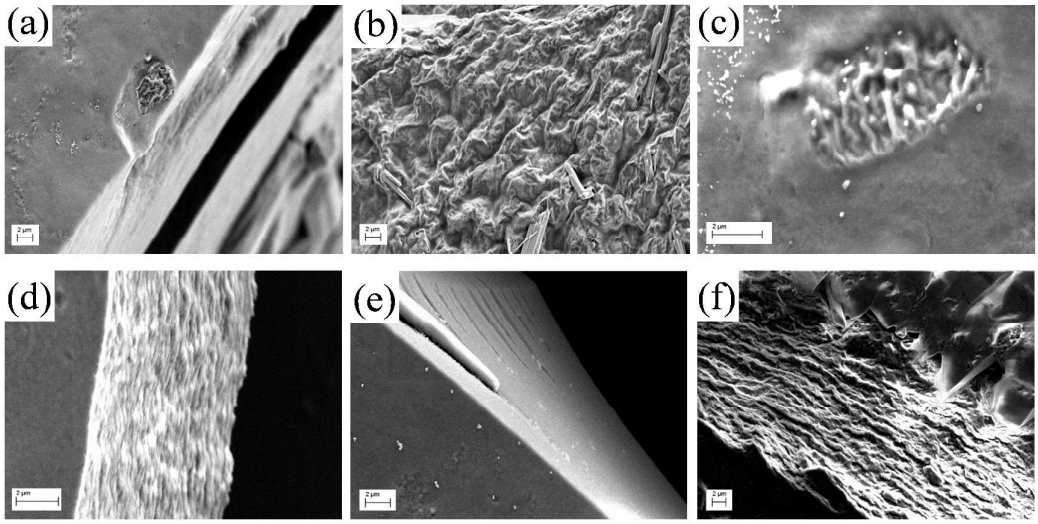

Figure 9. (a-f) SEM micrographs of 6 wt% ligand hydrogels dropcast onto silica wafers and dried *in vacuo* prior to imaging. **(e)** and **(c)** are coated, by sputtering, with Au to limit the effect of charging. Each bar represents 2μm.

SEM micrographs of the ligand gels are shown in Figure 9, after drop-casting the hydrogels onto silica wafers, followed by drying *in vacuo* prior to imaging. The SEM imaging demonstrated that the materials dried into compact solids with smooth surface texture, as demonstrated in Figure 9a. However, 'wrinkled surface' morphology, resembling a fibrous network of intertwined strands, was also observed in 10 % w/w samples, as shown in Figure 9b. Upon magnification of these surface gel features, it was possible to probe the morphology of the internal structure as shown in Figure 9a and 9c. These showed that the smooth gel surface was broken, through cratering or cracking, to give edges. Moreover, a variation in morphology was observed for the interior of the material, Figure 9d. Edges were observed throughout the gel, as shown in Figure 9d, where evidence of layering of the material was observed, Figure 9e. The edges of these layers appeared thick and fibrous (Figure 9d) consistent with the morphology of the material observed underneath the surface of the material. The smooth surface may reflect the material compacting due to the collapse of weak gel at the surface when solvent evaporation occurred in sample preparation, as thick entangled, fibre-like features were observed beneath the smooth surface, consistent with the theory of "surfactant-gel" materials formation from amphiphilic structures, where larger hydrophobically-driven self-assemblies compact into "spaghetti-like" assemblies, or long fibre-like extended networks, as shown in Figure 9a, and 9c. We believe that the entanglement of these within the matrix results in the formation of a gelating network.

This layered structure was reflected in the morphology throughout with consistent directionality seen in a number of features as pictured in Figure 9f. We are currently exploring the morphology of these are related structures in greater detail.

Conclusions

Herein, we have developed two new chiral ligands, based on the **dpa** motive, possessing chiral naphthyl chromophores/antennae, and explored their use in the formation of lanthanide directed synthesis of functional supramolecular structures and materials. The ligands were modified at the 4-position of the pyridyl unit to allow for the incorporation of a water-solubilising sulfonate centre; being the first examples of such chiral **dpa** structures that could be employed in pure water from our laboratory. These ligands were then used to generate complexes of Eu(III) in 1:3 (metal to ligand) stoichiometry under microwave irradiation, resulting in the formation of **Eu**·[**2**·*(R,R)*]$_3$ and **Eu**·[**2**·*(S,S)*]$_3$. Photophysical analysis of these in water or buffered water have showed that while only minor ligand based fluorescence was detected, metal centred Eu(III)-emission was apparent. In fact, the complexes **Eu**·[**2**·*(R,R)*]$_3$ and **Eu**·[**2**·*(S,S)*]$_3$ were highly luminescent with total quantum yield in water of *ca.* 14% for the lanthanide centred emission. This is significantly higher than that seen previously for such systems (*e.g.* **1**·*(R,R)* and **1**·*(S,S)*) in organic solutions. Moreover, in such highly competitive media, the antenna-to-ion energy transfer efficiency was also greatly improved; being *ca.* 80 %, almost three-fold that seen before. We propose that this enhancement is due to the amphilphilic nature of the ligand as well as hydrophobic effect; both clearly demonstrating the important role the functionalisation of the pyridyl unit has on the photophysical properties of the resulting systems. These complexes were also analysed using chiroptical spectroscopy, through the use of both CD and CPL. Both techniques confirmed that **Eu**·[**2**·*(R,R)*]$_3$ and **Eu**·[**2**·*(S,S)*]$_3$ were chiral and formed as pair of enantiomers (give rise to equal but opposite dichroism bands) where the chirality of the ligands was transferred to the complexes. The self-assembly between **2**·*(R,R)* or **2**·*(S,S)* with Eu(III) *in situ* was also investigated using changes in the absorption of the ligands as well as in the Eu(III) centred emission. From these changes we were able to probe both the various stoichiometries and their corresponding binding constants. Due to the relatively small changes seen in the absorption spectra, the changes in the CD spectra were also monitored and the changes quantified by using non-linear regression analysis. The results compared well with the changes observed in the ground and the excited states;

enabling more reliable quantification of the number of species in solution and their relative binding constants. These binding constants matched well with that seen in both the ground and from the Eu(III) excited state, confirming the use of this method to evaluate metal directed synthesis of supramolecular self-assemblies in solution, and the means of quantifying self-assembly processes through the probing of chiral properties though non-liner regression analysis. It was also observed that both **2**·*(R,R)* and **2**·*(S,S)* formed hydrogels in the presence of Cs_2CO_3 upon heating, that were stable towards a tube inversion test. Morphological analysis of these gels, using SEM imaging, showed that the ligands formed networks of layered material consisting of more complex fibrous networks that were intertwined underneath the smooth surface of the gel. The addition of Eu(III) to these gels, gave initially, red Eu(III) luminescent material or metallogels. However, the resulting Eu(III) complexes were not stable within the gel matrix, resulting in a phase-transition. We are currently exploring the rheology of these materials and use of other simple, chiral **dpa** ligands in the formation of novel functional lanthanide luminescent assemblies. We highlight and will further investigate the probing of chiroptical properties of Ln(III)-directed assembly in solution as a powerful method, complimenting routine achiral spectroscopy, to allow both stoichiometric speciation and binding affinities to be determined reliably from spectroscopic data.

Acknowledgements

We thank Dr. Oxana Kotova (TCD) for useful discussion and support. Drs. Joseph P. Byrne and Chris S. Hawes for proofreading the manuscript. This work was funded by Science Foundation Ireland (SFI) through the 2010 and 2013 Principle Investigator Award (10/IN.1/B2999 and 13/IA/1865; TG, SJB, AJS) and The President of Ireland Award (AJS). We thank Trinity College Dublin (TCD) and TCD School of Chemistry for a Postgraduate Scholarship (SJB)

Notes and References

[1] a) G. Gil-Ramírez, D. A. Leigh and A.J. Stephens, *Angew. Chem. Int. Ed*. 2015, **54**, 6110-6150. b) J. E. Beves, B. A. Blight, C. J. Campbell, D. A. Leigh and R. T. McBurney, *Angew. Chem. Int. Ed*. 2011, **50**, 9260-9327.

[2] D. A. Leigh, R. G. Pritchard and A. J. Stephens, *Nat. Chem*. 2014, **6**, 978-982.

[3] Tam, A.Y.-Y.; Yam, V.W.-W. *Chem. Soc. Rev.* **2013**, *42*, 1540-1567.

[4] (a) S. J. Bradberry, A. J. Savyasachi, M. Martinez-Calvo and T. Gunnlaugsson, *Coord. Chem. Rev.*, 2014, **273-274**, 226-241. (b) C. Lincheneau, F. Stomeo, S. Comby and T. Gunnlaugsson, *Aust. J. Chem.*, 2011, **64**, 1315-1326.

[5] R. S. Forgan, J.-P. Sauvage and J. F. Stoddart, *Chem. Rev*. 2011, **111**, 5434.

[6] a) J. A. Faiz, V. Heitz, and J. P. Sauvage, *Chem. Soc. Rev*., 2009, **38**, 422. b) M. C. T. Fyfe and J. F. Stoddart, *Acc. Chem. Res*. 1997, **30**, 393.

[7] C. O. Dietrich-Buchecker and J.-P. Sauvage, *Chem. Rev*. 1987, **87**, 795-810.

[8] S. Silvi, M. Venturi, and A. Credi *Chem. Commun*, 2011, **47**, 2483.

[9] S. M. Goldup, D. A. Leigh, P. J. Lusby, R. T. McBurney and A. M. Z. Slawin, *Angew. Chem. Int. Ed*. 2008, **47**, 6999.

[10] a) R. S. Forgan, J. J. Gassensmith, D. B. Cordes, M. M. Boyle, K. J. Hartlieb, D. C. Friedman, A. M. Z. Slawin, J. F. Stoddart, *J. Am. Chem. Soc*. 2012, **134**, 17007. c) H. Lahlali, K. Jobe, M. Watkinson, and S. M. Goldup, *Angew. Chem. Int. Ed*. 2011, **50**, 4151

[11] S. Comby, E. M. Surender, O. Kotova, L. K. Truman, J. K. Molloy and T. Gunnlaugsson, *Inorg. Chem*. 2014, **53**, 1867-1879 (And references therein).

[12] P. Ceroni, A. Credi and M. Venturi, *Chem. Soc. Rev.,* 2014, **43**, 4068-4083.

[13] J. P. Byrne, J. A. Kitchen, J. E. O'Brien, R. D. Peacock and T. Gunnlaugsson, *Inorg. Chem.* 2015, **54**, 1426-1439.

[14] J. Zhang and C.-Y. Su, *Coord. Chem. Rev*. 2013, **257**, 1373-1408. B) D.K. Kumar and J.W. Steed, *Chem. Soc. Rev*., 2014, **43,** 2080-2088. c) J. Zhang and C.-Y. Su, *Coord. Chem. Rev*. 2013, **257**, 1373-1408.

[15] a) J.-F. Ayme, G. Gil-Ramírez, D.A. Leigh, J.-F. Lemonnier, A. Markevicius, C.A. Muryn, G. Zhang, *J. Am. Chem. Soc.*, 2014, **136**, 13142-13145. b) J.-C. G. Bünzli, *Chem. Rev.*, 2010, **110**, 2729-2755. c) S. V. Eliseeva and J.-C. G. Bünzli, *New J. Chem.*, 2011, **35**, 1165-1176. d) M. C. Heffern, L. M. Matosziuk, and T. J. Meade, *Chem. Rev.*, 2014, **114**, 4496-4539. e) R. Carr, N. H. Evans and D. Parker, *Chem. Soc. Rev.*, 2012, **41**, 7673-7686. f) T. Le Borgne, P. Altmann, N. André, J.-C. G. Bünzli, G. Bernardinelli, P.-Y. Morgantini, J. Weber and C. Piguet, *Dalton Trans.*, 2004, 723-733. g) G. Canard, S. Koeller, G. Bernardinelli and C. Piguet *J. Am. Chem. Soc.*, 2008, **130**, 1025-1040. f) S.V. Eliseeva and J.-C. G. Bünzli, *Chem. Soc. Rev*. **2010**, *39*, 189-227.

[16] a) M. Cantuel, G. Bernardinelli, G. Muller, J.P. Riehl and C. Piguet *Inorg. Chem.*, 2004, **43**, 1840-1849; b) G. Bozoklu, C. Gateau, D. Imbert, J. Pécaut, K. Robeyns, Y.

Filinchuk, F. Memon, G. Muller and M. Mazzanti, *J. Am. Chem. Soc.*, 2012, **134**, 8372-8375; c) S. D. Bonsall, M. Houcheime, D. A. Straus and G. Muller, *Chem. Commun.*, 2007, 3676-3678; d) K. N. T. Hua, J. Xu, E. E. Quiroz, S. Lopez, A. J. Ingram, V. A. Johnson, A. R. Tisch, A. de Bettencourt-Dias, D. A. Straus and G. Muller, *Inorg. Chem.*, 2012, **51**, 647-660.

[17] a) W. J. Rieter, K. M. L. Taylor, H. Y. An, W. L. Lin and W. B. Lin, *J. Am. Chem. Soc.*, 2006, **128**, 9024. b) W. S. Liu, T. Q. Jiao, Y. Z. Li, Q. Z. Liu, M. Y. Tan, H. Wang and L. F. Wang, *J. Am. Chem. Soc.*, 2004, **126**, 2280.

[18] C. Butler, S. Goetz, C. M. Fitchett, P. E. Kruger and T. Gunnlaugsson, *Inorg. Chem.* 2011, **50**, 2723–2725.

[19] S. Zebret, E. Vçgele, T. Klumpler, and J. Hamacek, *Chem. Eur. J.* 2015, **21**, 6695-6699. b) J-C. G. Bünzli, *Acc. Chem. Res*., 2006, **39**, 53. c) J-C. G. Bünzli and C. Piguet *Chem. Soc. Rev*. 2005, **34**, 1048.

[20] a) J. Hamacek, in: *Metallofoldamers: Supramolecular Architectures from Helicates to Biomimetics*, Eds.: M. Albrecht, G. Mayaan, Wiley, New York, 2013, pp. 91-120. b) B. El Aroussi, S. Zebret, C. Besnard, P. Perrottet and J. Hamacek, *J. Am. Chem. Soc*. 2011, **133**, 10764–10767.

[21] a) R. Daly, O. Kotova, M. Boese, T. Gunnlaugsson and J. J. Boland, *ACS Nano* 2013, **7**, 4838-4845.b) O. Kotova, R. Daly, C.M.G. dos Santos, M. Boese, P.E. Kruger, J.J. Boland and T. Gunnlaugsson, T. *Angew. Chem. Int. Ed*. 2012, **51**, 7208-7212.

[22] a)C. Lincheneau, J. P. Leonard, T. McCabe and T. Gunnlaugsson, *Chem. Commun.*, 2011, **47**, 7119-7121. b) C. Lincheneau, C. Destribats, D. E. Barry, J. A. Kitchen, R. D. Peacock and T. Gunnlaugsson, *Dalton Trans.*, 2011, **40**, 12056-12059.

[23] O. Kotova, J. A. Kitchen, C. Lincheneau, R. D. Peacock and T. Gunnlaugsson, *Chem. Eur. J.*, 2013, **19**, 16181-16186.

[24] a) C. Lincheneau, R. D. Peacock and T. Gunnlaugsson, *Chem. Asian J.*, 2010, **5**, 500-504. B) F. Stomeo, C. Lincheneau, J. P. Leonard, J. E. O'Brien, R. D. Peacock, C. P. McCoy and T. Gunnlaugsson, *J. Am. Chem. Soc.*, 2009, **131**, 9636-9637. c) S. Comby, F. Stomeo, C. P. McCoy and T. Gunnlaugsson, *Helv. Chim. Acta*, 2009, **92**, 2461-2473.

[25] C. Lincheneau, B. Jean-Denis and T. Gunnlaugsson, *Chem. Commun.*, 2014, **50**, 2857-2860.

[26] M. Martínez-Calvo1, O. Kotova, M. E. Möbius, A. P. Bell, T. McCabe1, J. J. Boland and T. Gunnlaugsson, *J. Am. Chem. Soc.* 2015, **137**, 1983-1992.

[27] a) D. E. Barry, J. A. Kitchen, M. Albrecht, S. Faulkner and T. Gunnlaugsson, *Langmuir*, 2013, **29**, 11506-11515. b) J. A. Kitchen, D. E. Barry, L. Mercs, M. Albrecht, R.D. Peacock and T. Gunnlaugsson, *Angew. Chem. Int. Ed.*, 2012, **51**, 704-708.

[28] J. P. Leonard, P. Jensen, T. McCabe, J. E. O'Brien, R. D. Peacock, P.E. Kruger and T. Gunnlaugsson, *J. Am. Chem. Soc.*, 2007, **129**, 10986-10987.

[29] a) G. Muller, *Dalton Trans.*, 2009, 9692-9707. b) J. I. Bruce, D. Parker, S. Lopinski and R.D. Peacock, *Chirality*, 2002, **14**, 562-567.

[30] O. Kotova, S. Blasco, B. Twamley, J. E. O'Brien, R. D. Peacock, J. A. Kitchen, M. Martinez-Calvo and T. Gunnlaugsson, *Chem. Sci*., 2015, **6**, 457–471.

[31] S. G. Telfer, N. Tajima, R. Kuroda, M. Cantuel, and C. Piguet, *Inorg. Chem.* 2004, **43**, 5302-5310.

[32] *Comprehensive chiroptical spectroscopy*, ed. N. Berova, P. L. Polavarapu, K. Nakanishi and R. W. Woody, Wiley-VCH, New York, 2012.

[33] D. Wu and D. F. O'Shea, *Org. Lett.* **2013**, *15*, 3392.

[34] A. Beeby, I. M. Clarkson, R. S. Dickins, S. Faulkner, D. Parker, L. Royle, A. S. de Sousa, J. A. G. Williams and M. Woods, *J. Chem. Soc., Perkin Trans. 2*, 1999, 493-503.

[35] a) G. Pescitelli, L. Di Bari and N. Berova, *Chem. Soc. Rev.* 2014, **43**, 5211-5233. b) N. Berova, L. Di Bari and G. Pescitelli, *Chem. Soc. Rev.* 2007, **36**, 914-931. c) G. A. Hembury, V. V. Borovkov and Y. Inoue, *Chem. Rev.* 2008, **108**, 1-73.

[36] S. M. Cloonan, R. B. P. Elmes, M.-L. Erby, S. A. Bright, F. E. Poynton, D. E. Nolan, S. J. Quinn and T. Gunnlaugsson and D. Clive Williams, *J. Med. Chem.*, 2015 **DOI:** 10.1021/acs.jmedchem.5b00451.

[37] a) M. Albrecht, O. Osetska, T. Abel, G. Haberhauer and E. Ziegler, *Beilstein J. Org. Chem.* 2009, **78**, 1-8. b) SS. Sairenji, S. Akine and T. Nabeshima, *Tetrahedron Lett.* 2014, **55**, 1987-1990.